

# Constraining Selectron LSP Scenarios with Tevatron Trilepton Searches

H. K. Dreiner\*

*Bethe Center for Theoretical Physics and Physikalisches Institut, Universität Bonn, Bonn, Germany*

S. Grab†

*SCIPP, University of California Santa Cruz, Santa Cruz, CA 95064, USA*

T. Stefaniak‡

*Bethe Center for Theoretical Physics and Physikalisches Institut, Universität Bonn, Bonn, Germany and II. Physikalisches Institut, Universität Göttingen, Göttingen, Germany*

The Tevatron collaborations have searched for associated production of charginos and neutralinos via trilepton final states. No events above the Standard Model prediction were observed. We employ these results to put stringent bounds on  $R$ -parity violating models with a right-handed scalar electron as the lightest supersymmetric particle. We work in the framework of lepton number violating minimal supergravity. We find that within these models the complete parameter space consistent with the anomalous magnetic moment of the muon can be excluded at 90% confidence level. We also give prospects for Tevatron trilepton searches assuming an integrated luminosity of  $10 \text{ fb}^{-1}$ . We find that Tevatron will be able to test selectron LSP masses up to 170 GeV.

## I. INTRODUCTION

The LHC has been running for over a year and first searches for supersymmetry [1, 2] have been published [3–7]. In order to know what can possibly be expected at the LHC with present and forthcoming data, it is important to know the bounds implied by existing Tevatron searches [8–10]. It is our purpose here to investigate the bounds from Tevatron trilepton searches [11–16] on a specific supersymmetric scenario.

When extending the Standard Model (SM) of particle physics to include supersymmetry and implementing the minimal particle content, the supersymmetric Standard Model has more than 200 new parameters. Most of these arise from the supersymmetry breaking sector [1, 2]. In order to be able to perform phenomenological studies, usually simpler models are considered. We focus here on the baryon triality ( $B_3$ ) mSUGRA model [17, 18], where  $B_3$  is theoretically well motivated as an anomaly-free discrete gauge symmetry [19]. It has only 6 new parameters at the grand unification (GUT) scale ( $M_{\text{GUT}} = \mathcal{O}(10^{16} \text{ GeV})$ )

$$M_0, M_{1/2}, A_0, \tan\beta, \text{sgn}(\mu), \mathbf{\Lambda}. \quad (1)$$

Here,  $M_0$ ,  $M_{1/2}$  and  $A_0$  are the universal scalar mass, the universal gaugino mass and the universal trilinear scalar coupling, respectively.  $\tan\beta$  denotes the ratio of the two Higgs vacuum expectation values (vevs), and  $\text{sgn}(\mu)$  fixes the sign of the bilinear Higgs mass parameter  $\mu$ .  $\mathbf{\Lambda}$  is a lepton-number and  $R$ -parity violating parameter described below.

In  $B_3$  mSUGRA, the superpotential is extended by the lepton number violating (LNV) terms [20],

$$W_{\text{LNV}} = \frac{1}{2} \lambda_{ijk} L_i L_j \bar{E}_k + \lambda'_{ijk} L_i Q_j \bar{D}_k + \kappa_i L_i H_2, \quad (2)$$

which are absent in the minimal supersymmetric standard model (MSSM). Here,  $L_i$ ,  $Q_i$ ,  $H_2$ ,  $\bar{E}_i$  and  $\bar{D}_i$  are the standard MSSM chiral superfields.  $i, j, k$  are generation indices.  $\lambda_{ijk}$  and  $\lambda'_{ijk}$  are dimensionless couplings. The  $\kappa_i$  are dimensionful parameters, which vanish in  $B_3$  mSUGRA at  $M_{\text{GUT}}$  due to a redefinition of the lepton and Higgs superfields [17]. They are generated at lower scales via the renormalization group equations (RGEs), leading to interesting phenomenological consequences for neutrino masses [21, 22].

In the  $B_3$  mSUGRA model, we assume that exactly one of the thirty-six dimensionless couplings in Eq. (2) is non-zero and positive at the GUT scale. The parameter  $\mathbf{\Lambda}$  in Eq. (1) refers to this choice, *i.e.*

$$\mathbf{\Lambda} \in \{\lambda_{ijk}, \lambda'_{ijk}\}, \quad i, j, k = 1, 2, 3. \quad (3)$$

Given one coupling at  $M_{\text{GUT}}$ , other couplings that violate only the same lepton number are generated at the weak scale,  $M_Z$ , through the RGEs [17, 23–25].

An important feature of  $B_3$  mSUGRA models is that the lightest supersymmetric particle (LSP) is no longer stable. It is therefore not restricted to be electrically and color neutral [26]. Any supersymmetric particle can be the LSP. LNV interactions can significantly alter the RGE running of the sparticle masses such that we obtain new candidates for the LSP beyond the lightest neutralino,  $\tilde{\chi}_1^0$ , and lightest stau,  $\tilde{\tau}_1$  [27, 28]. We recently showed in detail in Ref. [29] that the interplay of a large magnitude of (negative)  $A_0$  with a  $L_i L_j \bar{E}_k$  coupling  $\mathbf{\Lambda} \gtrsim \mathcal{O}(10^{-2})$  can lead to a right-handed slepton LSP,  $\tilde{\ell}_R$ , of the first or second generation, *i.e.* to a selectron,  $\tilde{e}_R$ , or smuon,  $\tilde{\mu}_R$ , LSP. The

\* dreiner@th.physik.uni-bonn.de

† sgrab@scipp.ucsc.edu

‡ tim@th.physik.uni-bonn.de

$L_i L_j \bar{E}_k$	LSP candidate	$2\sigma$ bound
$\lambda_{121}, \lambda_{131}$	$\tilde{e}_R$	$0.020 \times (M_{\tilde{e}_R}/100 \text{ GeV})$
$\lambda_{231}$	$\tilde{e}_R$	$0.033 \times (M_{\tilde{e}_R}/100 \text{ GeV})$
$\lambda_{132}$	$\tilde{\mu}_R$	$0.020 \times (M_{\tilde{\mu}_R}/100 \text{ GeV})$

TABLE I. List of  $L_i L_j \bar{E}_k$  couplings (first column) needed to generate a  $\tilde{e}_R$ - or  $\tilde{\mu}_R$ -LSP (second column). The third column gives the most recent experimental bounds [95% confidence level (C.L.)], taken from Ref. [30]. The bounds apply at  $M_{\text{GUT}}$ .

respective  $L_i L_j \bar{E}_k$  couplings are given in Table I with their most recent  $2\sigma$  upper bounds [30] at  $M_{\text{GUT}}$ .

We also showed in Ref. [29] that our  $\tilde{\ell}_R$  LSP scenarios naturally lead to multi-lepton final states at hadron colliders. We found that the LHC can test large regions of the  $\tilde{\ell}_R$  LSP parameter space even with first data. These promising results have motivated us to investigate the present bounds on our model from Tevatron trilepton searches [8–10]: this is the topic of this paper. To be specific, we will concentrate on selectron LSP scenarios, where  $\lambda_{231}$  is the dominant  $R$ -parity violating coupling at  $M_{\text{GUT}}$ . Due to the weaker experimental bound on  $\lambda_{231}$ , *cf.* Table I, we can obtain a lighter sparticle mass spectrum resulting in larger cross sections for sparticle pair production at the Tevatron.

We find that the Tevatron rules out the  $\tilde{e}_R$  LSP parameter space within  $B_3$  mSUGRA, which is consistent with the anomalous magnetic moment of the muon within 2 standard deviations<sup>1</sup>. One should thus also consider going beyond  $B_3$  mSUGRA. We extrapolate the existing Tevatron analysis to an integrated luminosity of  $10 \text{ fb}^{-1}$  and find that more statistics can highly improve the sensitivity for heavier models. We therefore hope to encourage the Tevatron collaborations to search for our models in their upcoming trilepton supersymmetry (SUSY) searches.

This paper is organized as follows. In Sec. II, we review the  $\tilde{e}_R$  LSP parameter space relevant for our analysis and develop two benchmark scenarios for the Tevatron. We then apply in Sec. III the most recent  $D\bar{O}$  trilepton search [8] to the benchmark points and show the  $\tilde{e}_R$  LSP parameter space excluded by the Tevatron. In Sec. IV, we give prospects for future Tevatron analyses. We conclude in Sec. V. Appendix A presents the sparticle masses and branching ratios for our benchmark models.

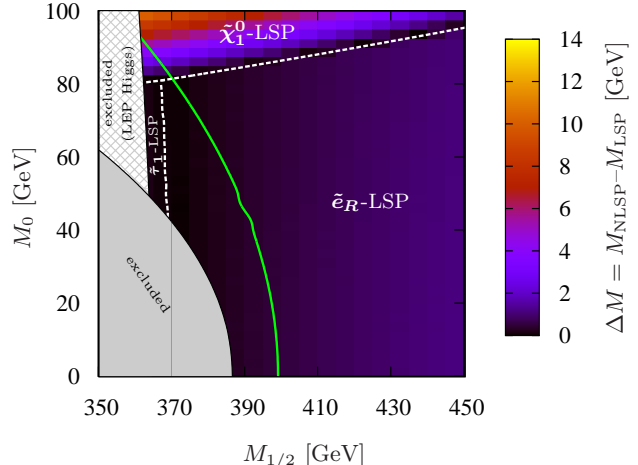


FIG. 1. Mass difference,  $\Delta M$ , between the next-to LSP (NLSP) and LSP in the  $M_{1/2} - M_0$  plane. The other  $B_3$  mSUGRA parameters are  $A_0 = -1250 \text{ GeV}$ ,  $\tan \beta = 5$ ,  $\text{sgn}(\mu) = +$  and  $\lambda_{231}|_{\text{GUT}} = 0.045$ . The LSP candidate regions are shown, bordered by the white dotted lines. The solid gray region on the bottom left is excluded due to the bound on  $\lambda_{231}$ , *cf.* Table I, and the patterned region in the top left is excluded by Higgs searches at LEP. The green contour line indicates the SUSY contribution to the anomalous magnetic moment of the muon,  $\delta a_\mu^{\text{SUSY}}$ . Models to the left lie within the  $2\sigma$  window for  $\delta a_\mu^{\text{SUSY}}$ , *cf.* Eq. (4).

## II. THE SELECTRON LSP IN $R$ -PARITY VIOLATING MSUGRA

### A. Selectron LSP Parameter Regions

The phenomenology and the typical parameter space of  $B_3$  mSUGRA models with a  $\tilde{e}_R$  or  $\tilde{\mu}_R$  LSP was discussed in detail in Ref. [29]. We review here the parameter space relevant for this work. In Fig. 1 we show a typical  $B_3$  mSUGRA parameter region with a  $\tilde{e}_R$  LSP in the  $M_{1/2} - M_0$  plane. We have chosen a fairly large negative value of  $A_0 = -1250 \text{ GeV}$ , in order to enhance the (negative) effect of  $\lambda_{231}$  on the RGE running of the  $\tilde{e}_R$  mass. The other parameters are  $\tan \beta = 5$ ,  $\text{sgn}(\mu) = +$  as well as  $\lambda_{231} = 0.045$  at the GUT scale. We can identify a  $\tilde{e}_R$ , a  $\tilde{\tau}_1$  and a  $\tilde{\chi}_1^0$  LSP region. The solid gray region at low values of  $M_{1/2}$  and  $M_0$  is excluded by the bound on the LNV coupling, *cf.* Table I. The green contour line indicates the lower value of the  $2\sigma$  window (using pion spectral functions from  $e^+e^-$  data<sup>2</sup>) of the SUSY contribution to the anomalous magnetic moment of the muon [33],

$$11.9 \times 10^{-10} < \delta a_\mu^{\text{SUSY}} < 47.1 \times 10^{-10}, \quad (4)$$

<sup>1</sup> The respective  $B_3$  mSUGRA parameter space with a  $\tilde{\mu}_R$  LSP is already ruled out by the stronger bound on  $\lambda_{132}$ , *cf.* Table I.

<sup>2</sup> Note that the SM prediction of  $a_\mu$  is consistent with observations if one uses spectral functions from  $\tau$  data [32].

B <sub>3</sub> mSUGRA parameter	SUSY1	SUSY2
$M_0$ [GeV]	0	80
$M_{1/2}$ [GeV]	400	375
$A_0$ [GeV]	-1250	-1250
$\tan\beta$	5	5
$\text{sgn}(\mu)$	+	+
$\lambda_{231} _{\text{GUT}}$	0.045	0.045

TABLE II. B<sub>3</sub> mSUGRA parameters for the benchmark points SUSY1 and SUSY2.

*i.e.* parameter points left of the green line lie within the  $2\sigma$  window and thus give a significant SUSY contribution to  $a_\mu$ . Furthermore, the entire displayed region fulfills the  $2\sigma$  constraints on the branching ratios of the decay  $b \rightarrow s\gamma$  [34],

$$3.03 \times 10^{-4} < \mathcal{B}(b \rightarrow s\gamma) < 4.07 \times 10^{-4}, \quad (5)$$

and the 95% C.L. upper limit on the flavor-changing-neutral-current (FCNC) decay  $B_s^0 \rightarrow \mu^+\mu^-$  [35],

$$\mathcal{B}(B_s^0 \rightarrow \mu^+\mu^-) < 3.6 \times 10^{-8}. \quad (6)$$

We also consider the bounds from Higgs searches at LEP on the light Higgs mass [36]. We employ `FeynHiggs2.7.4` [37] for the calculation of the Higgs mass, as well as its production and decay properties. The excluded supersymmetric parameter space provided by `HiggsBounds2.1.0` [38] is indicated as the patterned region in Fig. 1. We use `SOFTSUSY3.0.13` [39, 40] to calculate the SUSY spectrum and the Higgs mass parameters, and employ `micrOMEGAs2.2` [41] to calculate  $\mathcal{B}(b \rightarrow s\gamma)$ ,  $\mathcal{B}(B_s^0 \rightarrow \mu^+\mu^-)$  and  $\delta a_\mu^{\text{SUSY}}$ .

In this study, we focus on light  $\tilde{e}_R$  LSP models with an LSP mass  $M_{\text{LSP}} \lesssim 200$  GeV. A general feature of these scenarios is a near mass degeneracy<sup>3</sup> of the  $\tilde{e}_R$  LSP with the lightest stau,  $\tilde{\tau}_1$ . Thus, a large portion of the  $\tilde{e}_R$  LSP region exhibits a  $\tilde{\tau}_1$  NLSP. However, close to the  $\tilde{\chi}_1^0$  LSP region at larger values of  $M_0$ , we have  $\tilde{e}_R$  LSP scenarios with  $M_{\tilde{e}_R} \lesssim M_{\tilde{\chi}_1^0} \lesssim M_{\tilde{\tau}_1}$ , *i.e.* a  $\tilde{\chi}_1^0$  NLSP.

## B. Benchmark Scenarios for Tevatron Searches

In this section, we select two benchmark scenarios which we test explicitly against the DØ trilepton analysis described in the next section. The B<sub>3</sub> mSUGRA

parameters for the two benchmark points, denoted SUSY1 and SUSY2, are given in Table II. In both scenarios, the dominant  $R$ -parity violating coupling is  $\lambda_{231} = 0.045$  at  $M_{\text{GUT}}$ .

The benchmark point SUSY1 represents a wide region of the  $\tilde{e}_R$  LSP parameter space, where the mass difference between the  $\tilde{e}_R$  LSP and the lightest neutralino,  $\tilde{\chi}_1^0$ , is much larger than the mass difference between the  $\tilde{e}_R$  LSP and the  $\tilde{\tau}_1$  NLSP. The masses of the  $\tilde{e}_R$ ,  $\tilde{\tau}_1$  and  $\tilde{\chi}_1^0$  are 139.1 GeV, 139.6 GeV and 163.3 GeV, respectively. In fact, the next-to-NLSP (NNLSP) is the right-handed smuon,  $\tilde{\mu}_R$ , with a mass of 156.2 GeV. In contrast, SUSY2 lies in the boundary region to the  $\tilde{\chi}_1^0$  LSP. Here, all three sparticles  $\tilde{e}_R$ ,  $\tilde{\tau}_1$  and  $\tilde{\chi}_1^0$  are nearly degenerate in mass, with masses 151.5 GeV, 151.6 GeV and 152.8 GeV, respectively. Due to the low mass difference between  $\tilde{\chi}_1^0$  and  $\tilde{e}_R$ , we expect the electrons from the decay  $\tilde{\chi}_1^0 \rightarrow \tilde{e}_R e$  to be fairly soft, such that many do not fulfill the pre-selection criteria [29]. Detailed tables containing all sparticle masses and decay modes for these benchmark models are given in Appendix A. Both SUSY1 and SUSY2 are chosen such that they are on the edge of the  $2\sigma$  lower value of  $\delta a_\mu^{\text{SUSY}}$  (green line in Fig. 1).

## III. CONSTRAINTS FROM THE TEVATRON

At the Tevatron at Fermilab both experiments DØ [8] and CDF [9, 10] have searched<sup>4</sup> for supersymmetry with final states containing three charged leptons, using the collected data of proton-antiproton ( $p\bar{p}$ ) collisions at a center-of-mass energy  $\sqrt{s} = 1.96$  TeV, corresponding to an integrated luminosity of  $2.3 \text{ fb}^{-1}$  and  $3.2 \text{ fb}^{-1}$ , respectively. These analyses were designed for the measurement of associated production of charginos and neutralinos [48] within  $R$ -parity conserving mSUGRA, using exclusive trilepton search channels [11–16]. Some of our lighter models could have led to an observable excess of events in these searches. Here we investigate quantitatively how these experimental analyses constrain the  $\tilde{e}_R$  LSP parameter space.

We follow the DØ analysis to test the exclusion of  $\tilde{e}_R$  LSP models. CDF uses a jet veto in the event selection, which is expected to lead to a reduced signal efficiency for many  $\tilde{e}_R$  LSP models<sup>5</sup>. We therefore

<sup>3</sup> A larger mass difference between  $\tilde{e}_R$  and  $\tilde{\tau}_1$  can be obtained by increasing  $\Lambda$  and/or  $M_{1/2}$ . However, larger values of  $\Lambda$  translate into the need for larger  $\tilde{e}_R$  masses, *cf.* Table I. Thus, increasing either  $\Lambda$  or  $M_{1/2}$  leads to heavier scenarios, which we do not consider here.

<sup>4</sup> Note, that also other SUSY searches using the trilepton or (like-sign) dilepton signature have been performed at DØ and CDF [44–47]. At the current status, these analyses use at most a dataset corresponding to  $1.1 \text{ fb}^{-1}$ . Thus, we do not expect these searches to be more restrictive than those presented here.

<sup>5</sup> In order to discriminate the  $t\bar{t}$  background, CDF requires the scalar sum of the jet transverse energies  $\sum E_T(\text{jets}) \leq$

concentrate on the  $D\bar{O}$  search. Furthermore,  $D\bar{O}$  distinguishes their search channels by the flavor of the final state leptons. Since, in our models, the final state lepton flavor multiplicity depends on the choice of the  $\Lambda$  coupling, we expect different sensitivities of the  $D\bar{O}$  search channels for different choices of  $\Lambda$ .

In the next section we describe how we emulate the  $D\bar{O}$  analysis and discuss the major changes to the original analysis. We test the two  $\tilde{e}_R$  LSP benchmark points of Table II against our analysis in Sec. IIIB. We then review the results of the  $D\bar{O}$  analysis and show the excluded regions of the  $\tilde{e}_R$  LSP parameter space.

### A. The $D\bar{O}$ Trilepton Analysis

The  $D\bar{O}$  search for associated production of charginos and neutralinos with final states containing three charged leptons is presented in Ref. [8]. The analysis is based on  $p\bar{p}$  collision data at a center-of-mass energy of  $\sqrt{s} = 1.96$  TeV corresponding to an integrated luminosity of  $2.3 \text{ fb}^{-1}$ , with the exception of the analysis using identified hadronic  $\tau$  lepton decays, which is based on  $1 \text{ fb}^{-1}$  of data. Four dedicated trilepton event selections were designed, distinguished by the lepton content in the final state, *i.e.* we have a  $e\ell\ell$ ,  $\mu\mu\ell$ ,  $e\mu\ell$  and  $\mu\tau$  selection without specification of the lepton charge. Here the third lepton  $\ell$  corresponds to a reconstructed isolated track without using the  $D\bar{O}$  standard lepton identification criteria. The first three channels are separated into a low- $p_T$  and a high- $p_T$  selection, while the  $\mu\tau$  channel contains a  $\mu\tau\ell$  selection and a  $\mu\tau\tau$  selection. In this study, we focus on the  $e\ell\ell$ ,  $\mu\mu\ell$  and  $e\mu\ell$  channels. The  $\mu\tau$  selection turned out to be insensitive to our models.

In our object reconstruction, we use cone isolation criteria for all leptons, where the cone radius  $\Delta R = \sqrt{(\Delta\phi)^2 + (\Delta\eta)^2}$  is given by the distance in pseudorapidity  $\eta$  and azimuthal angle  $\phi$ . Guided by the  $D\bar{O}$  object reconstruction, an electron (muon<sup>6</sup>) with pseudorapidity  $|\eta| < 3.2$  ( $|\eta| < 2.0$ ) is considered as isolated, if the scalar sum of the absolute value of the transverse momenta of all tracks in a cone of  $\Delta R = 0.4$  does not exceed 2.5 GeV. We do not loosen the reconstruction criteria for the third lepton  $\ell$  but demand it to be an isolated electron or muon. Jets are reconstructed with **FastJet2.4.1** [50, 51] using the kt algorithm with  $R = 0.4$  and must be within  $|\eta| < 2.5$ . In our Monte Carlo (MC) simulation, the

missing transverse energy,  $\cancel{E}_T$ , is calculated as the sum over the transverse momenta of all invisible particles.

In the following, we describe the general features of the various steps in the event selection. The details are given in Table III and the specific values should be taken from this table. For a detailed description of the cuts and their effect on the SM background, we refer the reader again to Ref. [8].

First, each selection requires two identified leptons ( $\ell = e, \mu$ ) with certain minimum transverse momenta  $p_T^{\ell_1}, p_T^{\ell_2}$  (I). If more than two leptons are identified that satisfy the  $p_T$  criteria, the two leptons with the highest  $p_T$  are considered. Next, constraints on the invariant mass  $m_{\ell_1\ell_2}$  and the opening angle  $\Delta\phi_{\ell_1\ell_2}$  of the two leptons are imposed (II). This is followed in step (III) by requirements on  $\cancel{E}_T$ , the minimal transverse mass  $m_T^{\min} = \min(m_T^{\ell_1}, m_T^{\ell_2})$ , where

$$m_T^{\ell} = \sqrt{2p_T^{\ell}\cancel{E}_T[1 - \cos\Delta\phi(\ell, \cancel{E}_T)]}, \quad (7)$$

and  $H_T$ , which is the scalar sum of the  $p_T$  of all jets with  $p_T > 15$  GeV. In this step, a further requirement on  $\text{Sig}(\cancel{E}_T)$  is performed in the original  $D\bar{O}$  analysis, where  $\text{Sig}(\cancel{E}_T)$  is defined for events with at least one jet as

$$\text{Sig}(\cancel{E}_T) \equiv \frac{\cancel{E}_T}{\sqrt{\sum_{\text{jets}} \sigma^2(E_T^j || \cancel{E}_T)}}. \quad (8)$$

Here,  $\sigma^2(E_T^j || \cancel{E}_T)$  is the jet energy resolution projected on the  $\cancel{E}_T$  direction, *i.e.* on the direction of the missing transverse momentum vector.<sup>7</sup> This cut rejects events with  $\cancel{E}_T$  faked by poorly measured jets and thus significantly reduces the QCD background. In our approach, we do not apply this cut on  $\text{Sig}(\cancel{E}_T)$ , since we do not have a measure of the jet energy resolution. However, since the missing transverse energy stems mostly from the neutrinos coming from the leptonically decaying  $\tilde{e}_R$  LSP, the effect of this cut is expected to be small.

In step IV, we demand an additional third lepton with a softer  $p_T$  requirement. Further cuts on its transverse mass  $m_T^{\ell_3}$  and the invariant masses  $m_{\ell_1,2,\ell_3}$  of the third lepton with one of the preselected leptons are applied (V). For some channels in the original  $D\bar{O}$  analysis, step (VI) includes further lepton quality requirements using likelihood discriminants in order to reduce background from  $W$  boson production, where the second lepton is faked by jets or photons. This step is skipped in our approach, since this requires a more detailed simulation of the detector, beyond the scope of this work. In the last step (VII) we apply a

80 GeV and the number of jets  $N(\text{jets}) < 2$  [9]. We thus expect SUSY events from sparton (squark and/or gluino) pair production to be mostly rejected in the CDF analysis.

<sup>6</sup> This isolation criteria corresponds to *tight* muons in Ref. [8].

<sup>7</sup> Note that in Ref. [8] the symbol  $\vec{\cancel{E}}_T$  is used.

	Selection	$\mu\mu\ell$		$eel$		$e\mu\ell$	
		low $p_T$	high $p_T$	low $p_T$	high $p_T$	low $p_T$	high $p_T$
I	$p_T^{\ell_1}, p_T^{\ell_2}$	$> 12, > 8$	$> 18, > 16$	$> 12, > 8$	$> 20, > 10$	$> 12, > 8^a$	$> 15, > 15$
	$m_{\ell_1\ell_2}$	$\in [20, 60]$	$\in [0, 75]$	$\in [18, 60]$	$\in [0, 75]$	-	-
II	$\Delta\phi_{\ell_1\ell_2}$	$< 2.9$	$< 2.9$	$< 2.9$	$< 2.9$	-	-
	$\cancel{E}_T$	$> 20$	$> 20$	$> 22$	$> 20$	$> 20$	$> 20$
	$\text{Sig}(\cancel{E}_T)$	$> 8$	$> 8$	$> 8$	$> 8$	$> 8$	$> 8$
	$m_T^{\min}$	$> 20$	$> 20$	$> 20$	$> 14$	$> 20$	$> 15$
III	$H_T$	-	$< 80$	-	-	-	-
IV	$p_T^{\ell_3}$	$> 5$	$> 4$	$> 4$	$> 12$	$> 6$	$> 6$
	$m_T^{\ell_3}$	$> 10$	$> 10$	$> 10$	$> 10$	$> 10$	$> 8$
V	$m_{\ell_1,2\ell_3}$	$\notin [80, 110]$	-	-	-	$< 70$	$< 70$
	anti $W$	-	-	tight likelihood <sup>b</sup>	-	tight likelihood <sup>c</sup>	hit in 2 inner layers <sup>c</sup>
						very tight muon isolation <sup>d</sup>	
VI						$\sum_{0.05 < \Delta R < 0.4} p_T^{\ell_3} < 1$	
	$\cancel{E}_T \times p_T^{\ell_3}$	$> 200$	$> 300$	$> 220$	-	-	-
VII	$p_T^{\text{bal}}$	$< 4$	$< 4$	$< 4$	$< 4$	$< 2$	$< 2$

<sup>a</sup>  $p_T^{\ell_1}$  and  $p_T^{\ell_2}$  are electron and muon  $p_T$ , respectively.

<sup>b</sup> for  $p_T^{\ell_3} < 15$  GeV

<sup>c</sup> for  $m_T^{\mu} \in [40, 90]$  GeV

<sup>d</sup> for  $m_T^e \in [40, 90]$  GeV

TABLE III. DØ selection criteria for the  $\mu\mu\ell$ ,  $eel$  and  $e\mu\ell$  analyses for the low- $p_T$  selection and the high- $p_T$  selection, see text and Ref. [8] for further details. All energies, masses and momenta are in GeV, angles are in radians. We apply all cuts except the cut on  $\text{Sig}(\cancel{E}_T)$  in step III and the anti  $W$  requirements in step VI (both marked in gray).

cut on the product of the third lepton  $p_T$  and  $\cancel{E}_T$  as well as on the  $p_T$  balance

$$p_T^{\text{bal}} = \frac{|\vec{p}_T^{\ell_1} + \vec{p}_T^{\ell_2} + \vec{p}_T|}{p_T^{\ell_3}}. \quad (9)$$

## B. DØ Results and a Test of two Benchmark Scenarios

In order to test whether our benchmark models are excluded, we have generated 2000 signal events, *i.e.* the pair production of all SUSY particles, scaled to an integrated luminosity of  $2.3 \text{ fb}^{-1}$  and apply the simplified DØ analysis described above. We employ the Feldman & Cousins method [49] to set 90% C.L. upper limits given the number of expected background events and the number of observed events, both taken from the DØ paper [8]. In those cases where the number of observed events is smaller than the expected background, we take as the upper limit the 90% C.L. *sensitivity*, defined as the average upper limit that would be obtained by an ensemble of experiments with the expected background and no true signal, and given in

Signal cross section (in fb)	SUSY1	SUSY2
$\sigma(p\bar{p} \rightarrow \text{sarton pairs})$	$1.5 \pm 0.1$	$8.3 \pm 0.2$
$\sigma(p\bar{p} \rightarrow \text{slepton pairs})$	$8.5 \pm 0.2$	$6.5 \pm 0.1$
$\sigma\left(p\bar{p} \rightarrow \begin{array}{l} \text{gaugino pairs,} \\ \text{gaugino-sarton} \end{array}\right)$	$3.8 \pm 0.1$	$6.1 \pm 0.1$
$\sigma(p\bar{p} \rightarrow \text{sparticle pairs})$	$13.8 \pm 0.2$	$20.9 \pm 0.2$

TABLE IV. Leading-order (LO) signal cross sections for  $p\bar{p}$  collisions at a center-of-mass energy of  $\sqrt{s} = 1.96$  TeV for the benchmark scenarios SUSY1 and SUSY2. We give the cross section of sarton (*i.e.* squark and gluino) pair, slepton pair and electroweak (EW) gaugino pair / EW gaugino-sarton production separately. The last row gives the total sparticle pair production cross section, which is the signal process. We employed HERWIG6.510 to derive the LO cross sections and for the event simulation. The uncertainties are due to statistical fluctuations from HERWIG.

Table XII in Ref. [49]<sup>8</sup>. We claim a 90% C.L. exclusion

<sup>8</sup> For the number of expected background events  $> 15$ , we approximate the sensitivity by the Feldman & Cousins upper limit for  $N_{\text{obs}} = N_{\text{bkg}}$ . This is only relevant for the extrapolation to  $10 \text{ fb}^{-1}$  in Sec. IV.



Selection	$\mu\mu\ell$				$e\ell\ell$				$e\mu\ell$			
	Data	Backgrd.	SUSY1	SUSY2	Data	Backgrd.	SUSY1	SUSY2	Data	Backgrd.	SUSY1	SUSY2
I	194006	$195557 \pm 177$	6.6	17.8	235474	$232736 \pm 202$	19.8	11.7	16630	$16884 \pm 75$	12.6	18.2
II	22766	$26067 \pm 88$	1.4	4.2	31365	$27184 \pm 64$	4.8	2.8				
III	178	$181 \pm 6.4$	1.2	3.9	515	$212 \pm 12$	4.3	2.6	1191	$1177 \pm 20$	11.1	16.9
IV	7	$2.9 \pm 0.7$	1.0	2.8	16	$9.3 \pm 2.0$	3.0	1.3	22	$18.0 \pm 1.2$	9.9	11.0
V	4	$2.2 \pm 0.5$	0.6	2.4	9	$5.9 \pm 1.7$	2.8	1.3	3	$3.5 \pm 0.5$	3.8	3.9
VI					6	$3.1 \pm 0.4$			2	$1.6 \pm 0.4$		
VII	4	$1.2 \pm 0.2$	0.5	1.8	2	$1.8 \pm 0.2$	2.4	1.2	2	$0.8 \pm 0.2$	1.2	1.0

TABLE V. Numbers of events observed in the data and expected for the background (taken from Ref. [8]) and numbers of signal (SUSY1 and SUSY2, see text) events at various stages of the analysis for the  $\mu\mu\ell$ ,  $e\ell\ell$  and  $e\mu\ell$  channels and the low- $p_T$  selection. Each row corresponds to a group of cuts, as detailed in Table III. This is for an integrated luminosity of  $2.3 \text{ fb}^{-1}$ .

Selection	$\mu\mu\ell$				$e\ell\ell$				$e\mu\ell$			
	Data	Backgrd.	SUSY1	SUSY2	Data	Backgrd.	SUSY1	SUSY2	Data	Backgrd.	SUSY1	SUSY2
I	140417	$141781 \pm 120$	5.4	16.2	171001	$170197 \pm 175$	19.0	11.1	4617	$4709 \pm 23$	10.6	17.0
II	10349	$10645 \pm 51$	1.9	5.6	8273	$7937 \pm 39$	6.8	3.9				
III	173	$176 \pm 5.7$	1.2	3.7	244	$264 \pm 10$	6.4	3.8	727	$738 \pm 11$	9.8	16.0
IV	7	$3.8 \pm 0.5$	0.9	2.8	0	$1.5 \pm 0.3$	3.9	1.8	11	$12.7 \pm 0.9$	<b>8.8</b>	<b>10.3</b>
V	4	$2.9 \pm 0.4$	0.9	2.8	0	$1.1 \pm 0.3$	3.7	1.8	2	$2.8 \pm 0.5$	3.3	3.6
VI									0	$1.0 \pm 0.2$		
VII	4	$2.0 \pm 0.3$	0.9	2.4	0	$0.8 \pm 0.1$	<b>3.4</b>	1.7	0	$0.5 \pm 0.1$	0.9	1.0

TABLE VI. Same as Table V, but for the high- $p_T$  selection. Signal event yields that exceed the 90% C.L. upper exclusion bound are bold-face.

of the SUSY scenario, if the number of signal events exceeds this upper confidence limit in any step of the event selection. We do this comparison separately for all four<sup>9</sup> selection channels in order to gain some insight into their sensitivity to our models. Note that in this method, systematic uncertainties are not taken into account.

For the simulation, we use `SOFTSUSY3.0.13` [39, 40] to calculate the SUSY mass spectra. The `SOFTSUSY` output is fed into `ISAWIG1.200` and `ISAJET7.64` [52] in order to calculate the decay widths of the SUSY particles including the relevant  $R$ -parity violating decays. We have also added some missing three-body slepton decays to the `ISAJET` code; see Ref. [29] for details. The signal process, *i.e.* sparticle pair production, was simulated with `HERWIG6.510` [53–55].

For the two benchmark models, the leading-order (LO) cross sections of the following supersymmetric production processes are given in Table IV: sparton (*i.e.* squark and gluino) pair production, slepton pair production and electroweak (EW) gaugino pair as well as EW gaugino-sparton production. For the point SUSY1, sparticle production is dominated by slepton and gaugino production. In contrast, for SUSY2 the

sparton production dominates due to the low mass of the lightest stop,  $M_{\tilde{t}_1} = 304.9 \text{ GeV}$ , which decays exclusively to the lightest chargino and a bottom quark, *cf.* Table VIII. As a conservative approach, we only use the LO cross section for the signal, while the SM background in the  $D\bar{O}$  analysis [8] includes next-to-leading (NLO) and next-to-NLO corrections. Note, that higher order corrections usually enhance SUSY particle production at hadron colliders by several tens of percent [48, 56]. For the calculation of the Feldman & Cousins confidence limits we employ `ROOT` [57].

In Table V and Table VI, we review the results from the  $D\bar{O}$  analysis and compare them with the results for the two  $B_3$  mSUGRA models SUSY1 and SUSY2 for the low- $p_T$  and the high- $p_T$  selections, respectively.

In all selections, the signal event yield for both benchmark scenarios is  $\lesssim 20$  events after the two lepton requirement (step I) and for an integrated luminosity of  $2.3 \text{ fb}^{-1}$ . Thus, the event yields in the first steps (I-III) of the analysis are dominated by the overwhelming SM background. The analysis becomes sensitive to the signal once we require the third lepton (step IV and beyond). Then, the SM background is reduced to  $\mathcal{O}(1-20)$  expected events. We now discuss in detail the  $D\bar{O}$  results and the signal event yields of the different selections after step IV of the analysis was performed.

In the  $\mu\mu\ell$  channel (in both the low- $p_T$  and high- $p_T$  selection), the number of events observed by  $D\bar{O}$  is

<sup>9</sup> As mentioned before, the fourth channel including  $\tau$  leptons is insensitive. Thus we do not present the results for this specific channel here.

larger than the number of expected events from the SM background for all steps beyond cut IV. Therefore, this channel has intrinsically a less restrictive impact on the SUSY models. We expect only  $\mathcal{O}(1 - 3)$  signal events beyond step IV for both benchmark points. Hence, the  $\mu\mu\ell$  channel cannot exclude the SUSY1 and SUSY2 models.

Note, that SUSY2 yields roughly three times as many events in this selection as SUSY1. This is due to the enhanced  $\tilde{t}_1$  pair production and their decay to the lightest chargino, as mentioned above. The chargino decays to the  $\tilde{\nu}_\mu$  and a muon 21% of the time, leading to an enhanced number of muons in the signal. However, in the  $\mu\mu\ell$  high- $p_T$  selection, most of the signal events from sparton-pair production are rejected by the  $H_T$  cut in step III. This reduces in particular the SUSY2 event yield, since here the production of sparton-pairs comprises 40% of the signal cross section, *cf.* Table IV.

In the  $e\ell\ell$  channel, the number of observed events is larger (lower) than the number of expected SM background events in the low- $p_T$  (high- $p_T$ ) selection for all steps beyond cut IV. For both benchmark scenarios we expect  $\mathcal{O}(1 - 4)$  signal events in these steps of the analysis. Furthermore, the number of expected signal events for SUSY1 is roughly two times more than for SUSY2. This is because in SUSY2 the mass difference between the  $\tilde{\chi}_1^0$  and the  $\tilde{e}_R$  LSP is small. Therefore, the electrons from the decay  $\tilde{\chi}_1^0 \rightarrow \tilde{e}_R e$  tend to be soft and fail to pass the  $p_T$  criteria in step I of the  $e\ell\ell$  selection. The SUSY1 event yield exceeds the 90% C.L. upper bound in step VII of the high- $p_T$   $e\ell\ell$  selection and is therefore excluded by the  $D\bar{O}$  trilepton search.

For the low- $p_T$  selection of the  $e\mu\ell$  channel, the number of observed events tends to be larger than the number of expected SM background events, whereas in the high- $p_T$  selection, the number of observed events is slightly less. Both the SUSY1 and SUSY2 event yield exceed the 90% C.L. upper limit in step IV of the  $e\mu\ell$  high- $p_T$  selection. The following steps in the  $e\mu\ell$  channel (step V and beyond) are not as sensitive to our models as step IV, because the cut on the dilepton invariant masses in step V significantly reduces the signal.

In general, the  $B_3$  mSUGRA parameter region close to a  $\tilde{\chi}_1^0$  LSP is more difficult to exclude due to the soft electrons. For instance, in step IV of the  $e\mu\ell$  low- $p_T$  selection, the 90% C.L. upper limit is 13.0 events, while we expect 11.0 signal events for SUSY2. However, if we modify the  $M_0$  value of SUSY2 from 80 GeV to 75 GeV, *i.e.* we basically change the mass difference between  $\tilde{\chi}_1^0$  and  $\tilde{e}_R$  from 1.3 GeV to 3.7 GeV, the number of expected signal events increases to 15.2 events and the model is excluded.

We conclude, that the  $D\bar{O}$  analysis using  $2.3 \text{ fb}^{-1}$  of integrated luminosity excludes both benchmark points SUSY1 and SUSY2 at 90% C.L.. The most restrictive

channels for  $\tilde{e}_R$  LSP models with a dominant  $\lambda_{231}$  coupling are the  $e\ell\ell$  high- $p_T$  selection (in step VII) and the  $e\mu\ell$  high- $p_T$  selection (in step IV). In the next section, we determine the excluded regions of the  $\tilde{e}_R$  LSP parameter space.

### C. Excluded Selectron LSP Parameter Space

We now apply the  $D\bar{O}$  analysis to a more extensive  $\tilde{e}_R$  LSP parameter region. For this, we perform a scan in the  $M_{1/2} - M_0$  plane with  $M_{1/2} \in [350 \text{ GeV}, 500 \text{ GeV}]$  in steps of  $\Delta M_{1/2} = 5 \text{ GeV}$  and  $M_0 \in [0 \text{ GeV}, 120 \text{ GeV}]$  in steps of  $\Delta M_0 = 2.5 \text{ GeV}$ . We retain  $\lambda_{231} = 0.045$  at  $M_{\text{GUT}}$ . The other  $B_3$  mSUGRA parameter values are  $A_0 = -1250 \text{ GeV}$ ,  $\tan\beta = 5$  and  $\text{sgn}(\mu) = +$ . The scanned  $\tilde{e}_R$  LSP parameter region was already discussed in Sec. II A, *cf.* Fig. 1. For each parameter point with a  $\tilde{e}_R$  LSP, 2000 signal events were generated and scaled to an integrated luminosity of  $2.3 \text{ fb}^{-1}$ . Then the  $e\ell\ell$ ,  $\mu\mu\ell$  and  $e\mu\ell$  low- $p_T$  and high- $p_T$  event selections were applied<sup>10</sup>. At each step of the event selection, the number of passed events is compared with the  $D\bar{O}$  results as described above. We make this comparison for all event selection steps once the third lepton is required, *i.e.* for step IV and beyond, *cf.* Table III.

In the following figures, the patterned gray regions mark parameter points with either a neutralino or stau LSP (as indicated in the figures) which are not considered here. The solid gray region exhibits a LSP mass of  $M_{\tilde{e}_R} \lesssim 136 \text{ GeV}$  and is thus excluded by the bound on the  $\lambda_{231}$  coupling, *cf.* Table I. The mass of the  $\tilde{e}_R$  LSP (in GeV) is given by the gray contour lines.

In Fig. 2 we give the parameter region that is excluded at 90% C.L. with  $2.3 \text{ fb}^{-1}$  of analyzed data. We discuss each channel and  $p_T$  selection separately. Fig. 2(a) [Fig. 2(b)] shows the low- $p_T$  [high- $p_T$ ] selection of the  $e\ell\ell$  and  $e\mu\ell$  channel. The  $\mu\mu\ell$  channel does not exclude any  $\tilde{e}_R$  LSP parameter space.

The LSP decays to 50% to a (hard) muon and a neutrino. Thus, the  $e\mu\ell$  selection is very sensitive to these models and can exclude  $\tilde{e}_R$  LSP scenarios with  $\tilde{e}_R$  masses up to 150 GeV (155 GeV) and squark masses up to 850 GeV (880 GeV) with the low- $p_T$  (high- $p_T$ ) selection. The sensitivity decreases for lower mass differences of the  $\tilde{\chi}_1^0$  and the  $\tilde{e}_R$  due to the softer electrons, as can be seen in all displayed channels in Fig. 2(a) and Fig. 2(b). Especially the  $e\ell\ell$  channel becomes insensitive in this boundary region.

<sup>10</sup> We did the same for the  $\mu\tau$  selection for an integrated luminosity of  $1.0 \text{ fb}^{-1}$ . However, this channel is not capable of excluding any  $\tilde{e}_R$  LSP parameter space. Thus, we do not show any results for the  $\mu\tau$  channels.

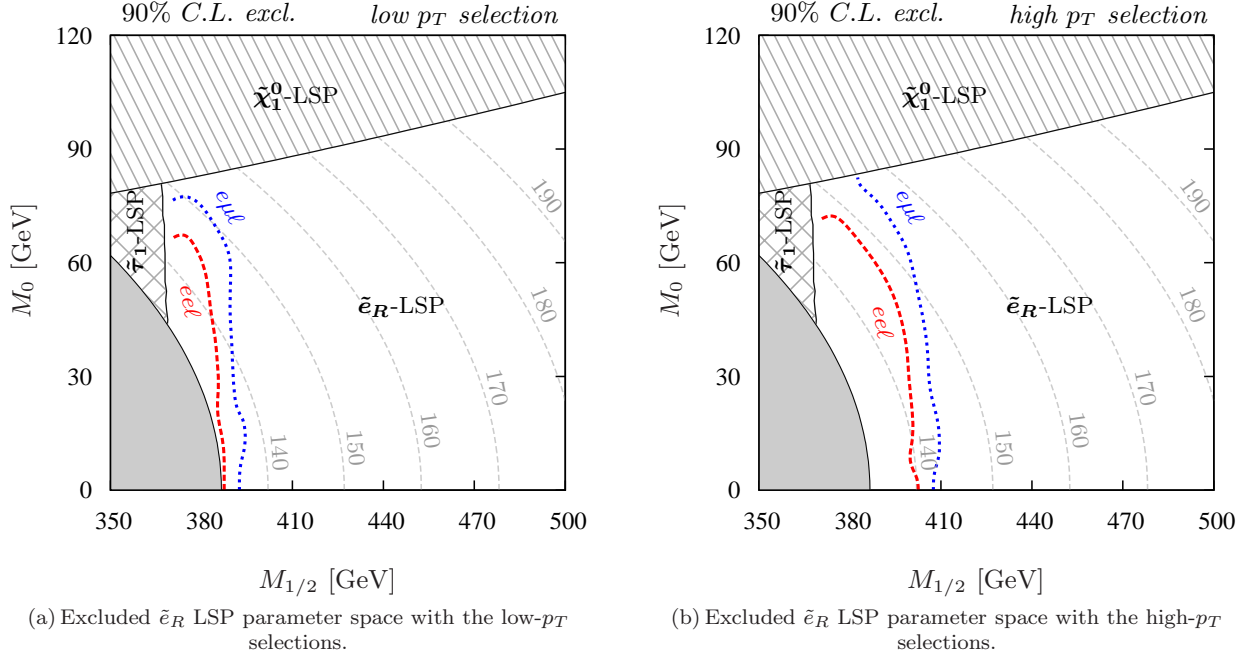


FIG. 2. Excluded regions (90% C.L.) of the  $\tilde{e}_R$  LSP parameter space by the DØ trilepton analysis with  $2.3 \text{ fb}^{-1}$  of data. We choose  $\lambda_{231} = 0.045$  as the dominant LNV coupling at  $M_{\text{GUT}}$ . The other parameters are  $A_0 = -1250 \text{ GeV}$ ,  $\tan \beta = 5$  and  $\text{sgn}(\mu) = +$ . The colored contour lines give the excluded region by the different channels: In Fig. 2(a) they correspond to the  $e\ell$  (red, dashed) and  $e\mu\ell$  (blue, dotted) low- $p_T$  selections, while in Fig. 2(b) they are shown for the same channels in the high- $p_T$  selection. The gray dotted contour lines give the LSP mass,  $M_{\tilde{e}_R}$ , in GeV, as indicated by the labels.

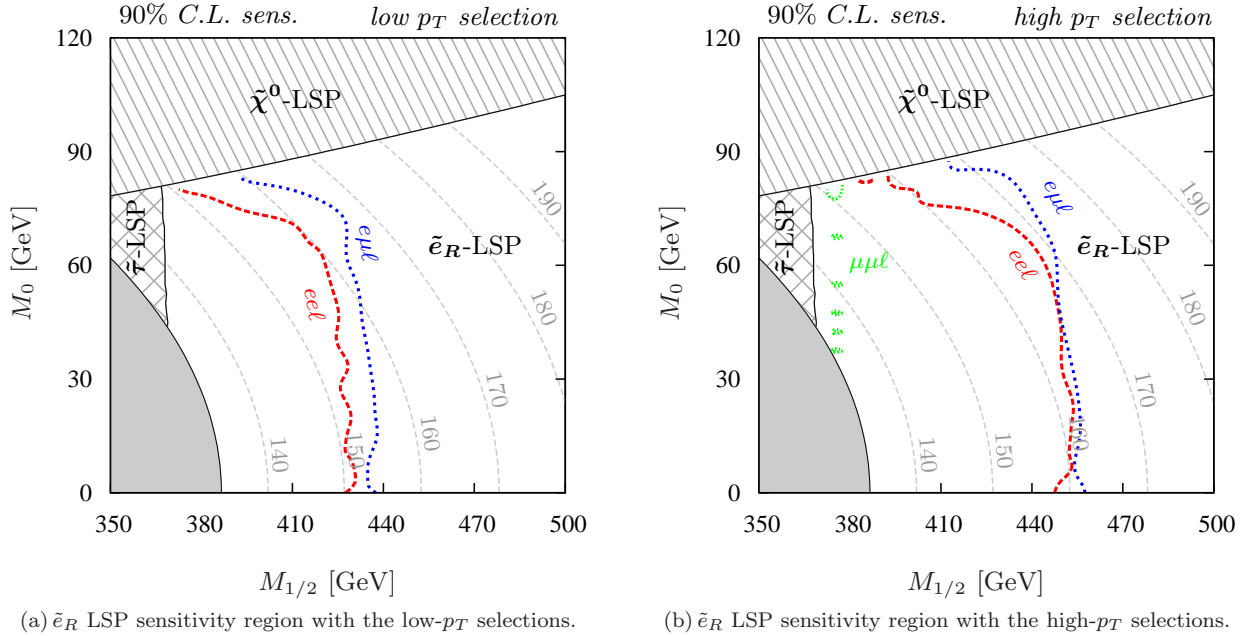


FIG. 3. Extrapolated sensitivity regions (90% C.L.) of the  $\tilde{e}_R$  LSP parameter space for the DØ trilepton analysis with future data corresponding to an integrated luminosity of  $10 \text{ fb}^{-1}$ . The parameter regions are the same as in Fig. 2. The colored contour lines give the sensitivity of the different channels: In Fig. 3(a) they correspond to the  $e\ell$  (red, dashed) and  $e\mu\ell$  (blue, dotted) low- $p_T$  selections, while in Fig. 3(b) they are shown for the same channels in the high- $p_T$  selection. Furthermore, the fine dotted, green contour line in Fig. 3(b) gives the sensitivity of the  $\mu\mu\ell$  high- $p_T$  selection. The gray dotted contour lines give the LSP mass,  $M_{\tilde{e}_R}$ , in GeV, as indicated by the labels.



Comparing the excluded  $\tilde{e}_R$  parameter region in Fig. 2 with Fig. 1, we conclude that  $\tilde{e}_R$  LSP scenarios with a significant contribution to the anomalous magnetic moment of the muon (region to the left of the green line in Fig. 1) are excluded at 90% C.L. by the DØ search with  $2.3 \text{ fb}^{-1}$  of analyzed data<sup>11</sup>.

#### IV. PROSPECTS FOR FUTURE TEVATRON SEARCHES

Both Tevatron experiments DØ and CDF acquired  $\sim 10 \text{ fb}^{-1}$  of data by the end of 2010. Therefore, we extrapolate the current DØ results to study the prospects of an exclusion of  $\tilde{e}_R$  LSP models, using data corresponding to an integrated luminosity of  $10 \text{ fb}^{-1}$ .

We assume that the events after each selection step in each channel are observed in the same rate as given by the results with integrated luminosity of  $2.3 \text{ fb}^{-1}$ , *cf.* Table V and Table VI. Then, we can extrapolate the data to the higher integrated luminosity of  $10 \text{ fb}^{-1}$ . By applying the same method as in the previous section, we determine the 90% C.L. sensitivity region, *i.e.* the supersymmetric parameter region which would lead to a significant deviation from the extrapolated data, assuming no discrepancies are observed.

In Fig. 3 we present the  $\tilde{e}_R$  LSP parameter space, which can potentially be excluded with a future integrated luminosity of  $10 \text{ fb}^{-1}$ . The parameter space is the same as in Fig. 2. The 90% C.L. sensitivity regions for the channels  $e\ell$ ,  $e\mu\ell$  and  $\mu\mu\ell$  are given by the contour lines for the low- $p_T$  (Fig. 3(a)) and high- $p_T$  (Fig. 3(b)) selection.

The most sensitive channels are the  $e\mu\ell$  and  $e\ell$  high- $p_T$  selections, which may exclude scenarios with  $M_{1/2} \lesssim 450 \text{ GeV}$  with future data, assuming no deviation from the SM prediction is observed. This corresponds to LSP masses  $M_{\tilde{e}_R} \lesssim (160 - 170) \text{ GeV}$  and squark masses  $M_{\tilde{q}} \lesssim (900 - 950) \text{ GeV}$ . As expected, the  $e\mu\ell$  selections are more efficient than the  $e\ell$  channels for scenarios with low mass difference between the  $\tilde{\chi}_1^0$  and the  $\tilde{e}_R$ . The  $\mu\mu\ell$  channel may become sensitive for models with  $M_{1/2} \approx (370 - 380) \text{ GeV}$ , because then the  $\tilde{t}_1$  decays dominantly via  $\tilde{t}_1 \rightarrow \tilde{\chi}_1^+ b$ , and the decay of the chargino leads to an enhanced muon multiplicity, *cf.* Table VIII. However, if the events are observed at the same rate as in the current data, the

$\mu\mu\ell$  channel will not play a major rôle in testing  $\tilde{e}_R$  LSP scenarios.

The DØ analysis used in this paper, was optimized for associated chargino and neutralino production within  $R$ -parity conserving supersymmetry. We point out, that larger regions of the selectron LSP parameter space (compared to this paper) can be investigated by the Tevatron collaborations if they optimize their cuts more towards our scenarios. For example, a harder cut on the muon transverse momentum will increase the signal to background ratio. In our models, the muons usually stem from the decay of the (heavy) selectron LSP into two Standard Model particles and thus have larger momenta. Similarly, a harder cut on  $\cancel{E}_T$  will help, since we have hard neutrinos stemming from the selectron or lightest stau decay and leading to a sizable amount of missing energy [29]. We point out that an *upper* cut on  $H_T$ , *i.e.* the scalar sum of the transverse momenta of all jets, should *not* be applied, because in large regions of the selectron LSP parameter space, sparton pair production, which leads to hard jets in the final state, occurs at a significant rate.

We conclude this section by pointing out, that the DØ analysis is sensitive to an extended  $\tilde{e}_R$  LSP parameter space with future data. Under the (strong) assumption, that we can linearly extrapolate the results given for an integrated luminosity of  $2.3 \text{ fb}^{-1}$  to a higher integrated luminosity,  $\tilde{e}_R$  LSP scenarios with  $M_{1/2} \lesssim 450 \text{ GeV}$  may be probed with  $10 \text{ fb}^{-1}$ .

#### V. SUMMARY AND CONCLUSION

A right-handed selectron is a natural candidate for the LSP within the B<sub>3</sub> mSUGRA model. If these or similar models are realized in nature, they usually produce a strong signal of multi charged lepton final states at hadron colliders like the Tevatron. On the one hand, each selectron LSP decay produces one hard charged lepton and missing energy. On the other hand, the decays of heavier SUSY particles into the selectron lead to additional charged leptons.

We have investigated the bounds on these models from the most recent DØ trilepton search (using an integrated luminosity of  $2.3 \text{ fb}^{-1}$ ). The non-observation of any events beyond the Standard Model expectation puts stringent bounds on our models. We found that scenarios with selectron LSP (squark) masses of up to 155 GeV (880 GeV) are excluded. We also found that the selectron LSP region consistent with the anomalous magnetic moment of the muon at  $2\sigma$  (using spectral functions from  $e^+e^-$  data) is ruled out by the DØ analysis. Thus, parameter regions outside B<sub>3</sub> mSUGRA should also be considered, for example, non-universal scalar masses.

We then extrapolated the DØ trilepton search to larger statistics, *i.e.* assuming an integrated luminos-

<sup>11</sup> The DØ search rules out all other regions of the B<sub>3</sub> mSUGRA parameter space with a  $\tilde{e}_R$  LSP consistent with  $a_\mu$  (beyond Fig. 1). For  $\tan\beta \lesssim 4$  these scenarios are ruled out by the LEP Higgs mass bounds. For  $\tan\beta \gtrsim 5.2$  the  $\tilde{\tau}_1$  is the LSP.  $A_0$  is strongly constrained by the requirements presented in Ref. [29] and  $\text{sgn}(\mu) = -$  is totally ruled out, because SUSY will then give a negative contribution to  $a_\mu$  [33]. If we go beyond B<sub>3</sub> mSUGRA then there is still a large parameter region with a  $\tilde{e}_R$  LSP allowed [29].

ity of  $10 \text{ fb}^{-1}$ . If no excess over the Standard Model expectations is observed, the Tevatron will be able to exclude selectron LSP models with a selectron (squark) mass of up to 170 GeV (950 GeV).

## ACKNOWLEDGMENTS

We thank John Conley, Klaus Desch, Sebastian Fleischmann and Peter Wienemann for helpful discussions. S.G. thanks the Alexander von Humboldt Foundation for financial support. The work of S.G. was also partly financed by the DOE grant DE-FG02-04ER41286. The work of H.K.D. was supported by the BMBF “Verbundprojekt HEP–Theorie” under the contract 05H09PDE and the Helmholtz Alliance “Physics at the Terascale”.

## Appendix A: Sparticle Masses and Branching Ratios of the Benchmark Models

The benchmark scenarios SUSY1 and SUSY2 possess a light sparticle mass spectrum. Therefore, the SUSY contribution to the anomalous magnetic moment of the muon,  $\delta a_\mu^{\text{SUSY}}$ , agrees within  $2\sigma$  with the discrepancy between the SM prediction and the observation, *cf.* Eq. (4). In both benchmark scenarios, SUSY1 and SUSY2, the  $\tilde{\tau}_1$  NLSP is nearly mass degenerate with the  $\tilde{e}_R$  LSP and exclusively undergoes

the  $R$ -parity violating decay  $\tilde{\tau}_1 \rightarrow e\tilde{\nu}_\mu$ . The electrons from this decay usually have a high momentum.

In Table VII, we give the sparticle mass spectrum and the dominant decay modes for SUSY1 ( $M_0 = 0 \text{ GeV}$ ,  $M_{1/2} = 400 \text{ GeV}$ ,  $A_0 = -1250 \text{ GeV}$ ,  $\tan\beta = 5$ ,  $\text{sgn}(\mu) = +$ ,  $\lambda_{231}|_{\text{GUT}} = 0.045$ ). The  $\tilde{e}_R$  LSP mass is about 139 GeV. Due to the low  $M_0$  value, the mass difference between the  $\tilde{\chi}_1^0$  next-to-NNLSP (NNNLSP) and the  $\tilde{e}_R$  LSP is about 24 GeV and thus fairly large. The right-handed smuon,  $\tilde{\mu}_R$ , is the NNLSP and undergoes three-body decays into the  $\tilde{e}_R$  LSP and  $\tilde{\tau}_1$  NLSP. These decays are discussed in detail in Ref. [29] and usually yield a low- $p_T$  muon. The lightest stop,  $\tilde{t}_1$ , has a mass of 366 GeV and decays preferably into the  $\tilde{\chi}_1^0$  and a  $t$  quark. The first and second generation squarks have masses around 820 – 860 GeV and the gluino mass is 934 GeV.

The sparticle mass spectrum and branching ratios of SUSY2 ( $M_0 = 80 \text{ GeV}$ ,  $M_{1/2} = 375 \text{ GeV}$ ,  $A_0 = -1250 \text{ GeV}$ ,  $\tan\beta = 5$ ,  $\text{sgn}(\mu) = +$ ,  $\lambda_{231}|_{\text{GUT}} = 0.045$ ) are given in Table VIII. This scenario lies near the  $\tilde{\chi}_1^0$  LSP region and thus the  $\tilde{\chi}_1^0$  NNLSP, the  $\tilde{\tau}_1$  NLSP and the  $\tilde{e}_R$  LSP have nearly degenerate masses around 152 GeV. We have a fairly light  $\tilde{t}_1$  with a mass of 305 GeV. The  $\tilde{t}_1$  decay into the  $\tilde{\chi}_1^0$  and a  $t$  quark is kinematically forbidden and  $\tilde{t}_1 \rightarrow \tilde{\chi}_1^\pm b$  is the only decay mode. The squarks of the first and second generation have masses around 780 – 820 GeV and the mass of the gluino is 881 GeV.

- 
- [1] H. P. Nilles, Phys. Rept. **110** (1984) 1-162.
  - [2] H. E. Haber, G. L. Kane, Phys. Rept. **117** (1985) 75-263.
  - [3] V. Khachatryan *et al.* [CMS Collaboration], [arXiv:1101.1628 [hep-ex]].
  - [4] ATLAS Collaboration, arXiv:1102.2357 [hep-ex].
  - [5] ATLAS Collaboration, arXiv:1102.5290 [hep-ex].
  - [6] CMS Collaboration, arXiv:1103.0953 [hep-ex].
  - [7] CMS Collaboration, arXiv:1103.1348 [hep-ex].
  - [8] V. M. Abazov *et al.* [D0 Collaboration], Phys. Lett. B **680**, 34 (2009) [arXiv:0901.0646 [hep-ex]].
  - [9] T. Aaltonen *et al.* [CDF Collaboration], Phys. Rev. Lett. **101**, 251801 (2008) [arXiv:0808.2446 [hep-ex]].
  - [10] R. Forrest [CDF Collaboration], arXiv:0910.1931 [hep-ex].
  - [11] H. Baer, K. Hagiwara and X. Tata, Phys. Rev. Lett. **57** (1986) 294.
  - [12] H. Baer, K. Hagiwara and X. Tata, Phys. Rev. D **35** (1987) 1598.
  - [13] V. D. Barger and C. Kao, Phys. Rev. D **60** (1999) 115015 [arXiv:hep-ph/9811489].
  - [14] K. T. Matchev and D. M. Pierce, Phys. Rev. D **60** (1999) 075004 [arXiv:hep-ph/9904282].
  - [15] H. Baer, M. Drees, F. Paige, P. Quintana and X. Tata, Phys. Rev. D **61** (2000) 095007 [arXiv:hep-ph/9906233].
  - [16] A. Dedes, H. K. Dreiner, U. Nierste, P. Richardson, [hep-ph/0207026].
  - [17] B. C. Allanach, A. Dedes, H. K. Dreiner, Phys. Rev. **D69** (2004) 115002. [hep-ph/0309196].
  - [18] B. C. Allanach, M. A. Bernhardt, H. K. Dreiner *et al.*, Phys. Rev. **D75** (2007) 035002. [hep-ph/0609263].
  - [19] H. K. Dreiner, C. Luhn, H. Murayama *et al.*, Nucl. Phys. **B795** (2008) 172-200. [arXiv:0708.0989 [hep-ph]]. L. E. Ibanez, G. G. Ross, Nucl. Phys. **B368** (1992) 3-37. T. Banks, M. Dine, Phys. Rev. **D45** (1992) 1424-1427. [hep-th/9109045].
  - [20] H. K. Dreiner, arXiv:hep-ph/9707435.
  - [21] B. C. Allanach, C. H. Kom, JHEP **0804** (2008) 081. [arXiv:0712.0852 [hep-ph]].
  - [22] H. K. Dreiner, M. Hahnussek, S. Grab, Phys. Rev. **D82** (2010) 055027. [arXiv:1005.3309 [hep-ph]].
  - [23] B. C. Allanach, A. Dedes and H. K. Dreiner, Phys. Rev. D **60**, 056002 (1999) [arXiv:hep-ph/9902251].
  - [24] H. K. Dreiner, S. Grab and M. K. Trenkel, Phys. Rev. D **79** (2009) 016002 [Erratum-ibid. **79** (2009) 019902] [arXiv:0808.3079 [hep-ph]].
  - [25] B. de Carlos and P. L. White, Phys. Rev. D **54** (1996) 3427 [arXiv:hep-ph/9602381].
  - [26] J. R. Ellis, J. S. Hagelin, D. V. Nanopoulos, K. A.

mass [GeV]	channel	BR	channel	BR
$\tilde{e}_R^-$ <b>139.1</b>	$\mu^- \nu_\tau$	<b>50%</b>	$\tau^- \nu_\mu$	<b>50%</b>
$\tilde{\tau}_1^-$ 139.6	$e^- \bar{\nu}_\mu$	<b>100%</b>		
$\tilde{\mu}_R^-$ 156.2	$\tilde{e}_R^+ e^- \mu^-$	30.2%	$\tilde{e}_R^- e^+ \mu^-$	25.1%
	$\tilde{\tau}_1^+ \tau^- \mu^-$	24.4%	$\tilde{\tau}_1^- \tau^+ \mu^-$	20.3%
$\tilde{\chi}_1^0$ 163.3	$\tilde{e}_R^+ e^+$	24.7%	$\tilde{e}_R^- e^-$	24.7%
	$\tilde{\tau}_1^- \tau^+$	22.9%	$\tilde{\tau}_1^+ \tau^-$	22.9%
	$\tilde{\mu}_R^- \mu^+$	2.4%	$\tilde{\mu}_R^+ \mu^-$	2.4%
$\tilde{\nu}_\tau$ <b>254.9</b>	$\tilde{\chi}_1^0 \nu_\tau$	63.9%	$W^+ \tilde{\tau}_1^-$	24.1%
	$e^- \mu^+$	<b>12.1%</b>		
$\tilde{\nu}_\mu$ <b>258.1</b>	$\tilde{\chi}_1^0 \nu_\mu$	84.5%	$e^- \tau^+$	<b>15.5%</b>
$\tilde{\nu}_e$ 262.9	$\tilde{\chi}_1^0 \nu_e$	100%		
$\tilde{\mu}_L^-$ <b>269.3</b>	$\tilde{\chi}_1^0 \mu^-$	84.2%	$e^- \bar{\nu}_\tau$	<b>15.8%</b>
$\tilde{\tau}_2^-$ <b>269.6</b>	$\tilde{\chi}_1^0 \tau^-$	63.7%	$H^0 \tilde{\tau}_1^-$	13.1%
	$\tilde{\chi}_1^0 \tilde{\tau}_1^-$	12.8%	$e^- \bar{\nu}_\mu$	<b>10.5%</b>
$\tilde{e}_L^-$ 273.9	$\tilde{\chi}_1^0 e^-$	100%		
$\tilde{\chi}_2^0$ 311.1	$\tilde{\nu}_\tau \nu_\tau$	10.8%	$\tilde{\nu}_\tau \nu_\tau$	10.8%
	$\tilde{\nu}_\mu \nu_\mu$	9.7%	$\tilde{\nu}_\mu \nu_\mu$	9.7%
	$\tilde{\nu}_e \nu_e$	8.1%	$\tilde{\nu}_e \nu_e$	8.1%
	$\tilde{\mu}_L^- \mu^+$	6.6%	$\tilde{\mu}_L^+ \mu^-$	6.6%
	$\tilde{\tau}_2^- \tau^+$	6.3%	$\tilde{\tau}_2^+ \tau^-$	6.3%
	$\tilde{e}_L^- e^+$	5.4%	$\tilde{e}_L^+ e^-$	5.4%
	$\tilde{\tau}_1^- \tau^+$	2.7%	$\tilde{\tau}_1^+ \tau^-$	2.7%
$\tilde{\chi}_1^-$ 311.2	$\tilde{\nu}_\tau \tau^-$	22.3%	$\tilde{\nu}_\mu \mu^-$	20.0%
	$\tilde{\nu}_e e^-$	16.9%	$\tilde{\mu}_L^- \bar{\nu}_\mu$	12.7%
	$\tilde{\tau}_2^- \bar{\nu}_\tau$	12.1%	$\tilde{e}_L^- \bar{\nu}_e$	10.3%
	$\tilde{\tau}_1^- \bar{\nu}_\tau$	5.0%		
$\tilde{t}_1$ 365.8	$\tilde{\chi}_1^0 t$	69.1%	$\tilde{\chi}_1^+ b$	30.9%
$\tilde{b}_1$ 706.3	$W^- \tilde{t}_1$	78.5%	$\tilde{\chi}_1^- t$	12.8%
	$\tilde{\chi}_2^0 b$	8.2%		
$\tilde{t}_2$ 790.6	$Z^0 \tilde{t}_1$	55.3%	$H^0 \tilde{t}_1$	22.9%
	$\tilde{\chi}_1^+ b$	14.3%	$\tilde{\chi}_2^0 t$	1.2%
$\tilde{\chi}_3^0$ 819.8	$\tilde{t}_1 \bar{t}$	26.5%	$\tilde{t}_1^* t$	26.5%
	$\tilde{\chi}_1^- W^+$	14.2%	$\tilde{\chi}_1^+ W^-$	14.2%
	$\tilde{\chi}_2^0 Z^0$	12.6%	$\tilde{\chi}_1^0 Z^0$	3.7%
	$\tilde{\chi}_2^0 H^0$	1.0%		
$\tilde{b}_2$ 821.5	$\tilde{\chi}_1^0 b$	59.3%	$W^- \tilde{t}_1$	36.8%
	$\tilde{\chi}_1^- t$	2.0%	$\tilde{\chi}_2^0 b$	1.2%
$\tilde{d}_R (\bar{s}_R)$ 824.2	$\tilde{\chi}_1^0 d(s)$	100%		
$\tilde{u}_R (\bar{c}_R)$ 826.3	$\tilde{\chi}_1^0 u(c)$	100%		
$\tilde{\chi}_2^-$ 828.0	$\tilde{t}_1^* b$	57.5%	$\tilde{\chi}_2^0 W^-$	12.9%
	$\tilde{\chi}_1^- Z^0$	12.4%	$\tilde{\chi}_1^- H^0$	11.6%
	$\tilde{\chi}_1^0 W^-$	3.3%		
$\tilde{\chi}_4^0$ 828.3	$\tilde{t}_1 \bar{t}$	34.7%	$\tilde{t}_1^* t$	34.7%
	$\tilde{\chi}_1^- W^+$	9.0%	$\tilde{\chi}_1^+ W^-$	9.0%
	$\tilde{\chi}_2^0 H^0$	7.5%	$\tilde{\chi}_1^0 H^0$	2.2%
$\tilde{u}_L (\bar{c}_L)$ 856.3	$\tilde{\chi}_1^+ d(s)$	65.9%	$\tilde{\chi}_2^0 u(c)$	32.9%
	$\tilde{\chi}_1^0 u(c)$	1.2%		
$\tilde{d}_L (\bar{s}_L)$ 859.8	$\tilde{\chi}_1^- u(c)$	65.5%	$\tilde{\chi}_2^0 d(s)$	32.8%
	$\tilde{\chi}_1^0 d(s)$	1.7%		
$\tilde{g}$ 933.8	$\tilde{t}_1 \bar{t}$	23.4%	$\tilde{t}_1^* t$	23.4%
	$\tilde{b}_1 \bar{b}$	9.2%	$\tilde{b}_1^* b$	9.2%
	$\tilde{b}_2 \bar{b}$	2.6%	$\tilde{b}_2^* b$	2.6%
	$\tilde{d}_R \bar{d}(\bar{s}_R \bar{s})$	2.5%	$\tilde{d}_R^* d(\bar{s}_R^* s)$	2.5%
	$\tilde{u}_R \bar{u}(\bar{c}_R \bar{c})$	2.4%	$\tilde{u}_R^* u(\bar{c}_R^* c)$	2.4%
	$\tilde{u}_L \bar{u}(\bar{c}_L \bar{c})$	1.3%	$\tilde{u}_L^* u(\bar{c}_L^* c)$	1.3%
	$\tilde{d}_L \bar{d}(\bar{s}_L \bar{s})$	1.2%	$\tilde{d}_L^* d(\bar{s}_L^* s)$	1.2%

TABLE VII. Branching ratios (BRs) and sparticle masses for the benchmark scenario SUSY1. BRs smaller than 1% are neglected.  $R$ -parity violating decays are shown in bold-face. Masses which are reduced by more than 5 GeV (compared to the  $R$ -parity conserving spectrum) due to  $\lambda_{231}|_{\text{GUT}} = 0.045$  are also shown in bold-face.

mass [GeV]	channel	BR	channel	BR
$\tilde{e}_R^-$ <b>151.5</b>	$\mu^- \nu_\tau$	<b>50%</b>	$\tau^- \nu_\mu$	<b>50%</b>
$\tilde{\tau}_1^-$ 151.6	$e^- \bar{\nu}_\mu$	<b>100%</b>		
$\tilde{\chi}_1^0$ 152.8	$\tilde{e}_R^- e^+$	50.0%	$\tilde{e}_R^+ e^-$	50%
$\tilde{\mu}_R^-$ 167.3	$\tilde{\chi}_1^0 \mu^-$	100%		
$\tilde{\nu}_\tau$ <b>250.4</b>	$\tilde{\chi}_1^0 \nu_\tau$	75.7%	$e^- \mu^+$	<b>12.6%</b>
	$W^+ \tilde{\tau}_1^-$	11.7%		
$\tilde{\nu}_\mu$ <b>253.7</b>	$\tilde{\chi}_1^0 \nu_\mu$	86.1%	$e^- \tau^+$	<b>13.9%</b>
$\tilde{\nu}_e$ 258.5	$\tilde{\chi}_1^0 \nu_e$	100%		
$\tilde{\mu}_L^-$ <b>265.0</b>	$\tilde{\chi}_1^0 \mu^-$	85.5%	$e^- \bar{\nu}_\tau$	<b>14.5%</b>
$\tilde{\tau}_2^-$ <b>265.6</b>	$\tilde{\chi}_1^0 \tau^-$	80.6%	$e^- \bar{\nu}_\mu$	<b>11.6%</b>
	$Z^0 \tilde{\tau}_1^-$	7.7%		
$\tilde{e}_L^-$ 269.6	$\tilde{\chi}_1^0 e^-$	100%		
$\tilde{\chi}_2^0$ 291.0	$\tilde{\nu}_\tau \nu_\tau$	12.0%	$\tilde{\nu}_\tau \nu_\tau$	12.0%
	$\tilde{\nu}_\mu \nu_\mu$	10.3%	$\tilde{\nu}_\mu \nu_\mu$	10.3%
	$\tilde{\nu}_e \nu_e$	7.9%	$\tilde{\nu}_e \nu_e$	7.9%
	$\tilde{\mu}_L^- \mu^+$	5.5%	$\tilde{\mu}_L^+ \mu^-$	5.5%
	$\tilde{\tau}_2^- \tau^+$	5.0%	$\tilde{\tau}_2^+ \tau^-$	5.0%
	$\tilde{\tau}_1^- \tau^+$	4.7%	$\tilde{\tau}_1^+ \tau^-$	4.7%
	$\tilde{e}_L^- e^+$	3.8%	$\tilde{e}_L^+ e^-$	3.8%
	$\tilde{\chi}_1^0 H^0$	1.0%		
$\tilde{\chi}_1^-$ 291.0	$\tilde{\nu}_\tau \tau^-$	24.8%	$\tilde{\nu}_\mu \mu^-$	21.3%
	$\tilde{\nu}_e e^-$	16.4%	$\tilde{\mu}_L^- \bar{\nu}_\mu$	10.5%
	$\tilde{\tau}_2^- \bar{\nu}_\tau$	9.6%	$\tilde{\tau}_1^- \bar{\nu}_\tau$	8.9%
	$\tilde{e}_L^- \bar{\nu}_e$	7.2%	$\tilde{\chi}_1^0 W^-$	1.0%
$\tilde{t}_1$ 304.9	$\tilde{\chi}_1^+ b$	100%		
$\tilde{b}_1$ 661.6	$W^- \tilde{t}_1$	80.9%	$\tilde{\chi}_1^- t$	11.2%
	$\tilde{\chi}_2^0 b$	7.5%		
$\tilde{t}_2$ 750.2	$Z^0 \tilde{t}_1$	57.1%	$H^0 \tilde{t}_1$	22.2%
	$\tilde{\chi}_1^+ b$	13.2%	$\tilde{\chi}_2^0 t$	5.4%
	$\tilde{\chi}_1^0 t$	1.2%		
$\tilde{b}_2$ 779.1	$\tilde{\chi}_1^0 b$	56.7%	$W^- \tilde{t}_1$	39.3%
	$\tilde{\chi}_1^- t$	1.9%	$\tilde{\chi}_2^0 b$	1.2%
$\tilde{d}_R (\bar{s}_R)$ 781.9	$\tilde{\chi}_1^0 d(s)$	100%		
$\tilde{u}_R (\bar{c}_R)$ 783.7	$\tilde{\chi}_1^0 u(c)$	100%		
$\tilde{\chi}_3^0$ 793.9	$\tilde{t}_1 \bar{t}$	28.5%	$\tilde{t}_1^* t$	28.5%
	$\tilde{\chi}_1^- W^+$	13.0%	$\tilde{\chi}_1^+ W^-$	13.0%
	$\tilde{\chi}_2^0 Z^0$	11.4%	$\tilde{\chi}_1^0 Z^0$	3.3%
	$\tilde{\chi}_2^0 H^0$	1.0%		
$\tilde{\chi}_2^-$ 802.1	$\tilde{t}_1^* b$	60.4%	$\tilde{\chi}_2^0 W^-$	11.9%
	$\tilde{\chi}_1^- Z^0$	11.5%	$\tilde{\chi}_1^- H^0$	10.7%
	$\tilde{\chi}_1^0 W^-$	3.0%		
$\tilde{\chi}_4^0$ 802.4	$\tilde{t}_1 \bar{t}$	36.1%	$\tilde{t}_1^* t$	36.1%
	$\tilde{\chi}_1^- W^+$	8.2%	$\tilde{\chi}_1^+ W^-$	8.2%
	$\tilde{\chi}_2^0 H^0$	6.7%	$\tilde{\chi}_1^0 H^0$	2.0%
$\tilde{u}_L (\bar{c}_L)$ 811.4	$\tilde{\chi}_1^+ d(s)$	66.0%	$\tilde{\chi}_2^0 u(c)$	33.0%
	$\tilde{\chi}_1^0 u(c)$	1.0%		
$\tilde{d}_L (\bar{s}_L)$ 815.0	$\tilde{\chi}_1^- u(c)$	65.5%	$\tilde{\chi}_2^0 d(s)$	32.8%
	$\tilde{\chi}_1^0 d(s)$	1.7%		
$\tilde{g}$ 881.0	$\tilde{t}_1 \bar{t}$	24.7%	$\tilde{t}_1^* t$	24.7%
	$\tilde{b}_1 \bar{b}$	9.5%	$\tilde{b}_1^* b$	9.5%
	$\tilde{b}_2 \bar{b}$	2.4%	$\tilde{b}_2^* b$	2.4%
	$\tilde{d}_R \bar{d}(\bar{s}_R \bar{s})$	2.3%	$\tilde{d}_R^* d(\bar{s}_R^* s)$	2.3%
	$\tilde{u}_R \bar{u}(\bar{c}_R \bar{c})$	2.2%	$\tilde{u}_R^* u(\bar{c}_R^* c)$	2.2%
	$\tilde{u}_L \bar{u}(\bar{c}_L \bar{c})$	1.2%	$\tilde{u}_L^* u(\bar{c}_L^* c)$	1.2%
	$\tilde{d}_L \bar{d}(\bar{s}_L \bar{s})$	1.1%	$\tilde{d}_L^* d(\bar{s}_L^* s)$	1.1%

TABLE VIII. Same as Table VII, but for the benchmark point SUSY2.

- Olive, M. Srednicki, Nucl. Phys. **B238** (1984) 453-476.
- [27] M. A. Bernhardt, S. P. Das, H. K. Dreiner, S. Grab, Phys. Rev. **D79** (2009) 035003. [arXiv:0810.3423 [hep-ph]].
  - [28] H. K. Dreiner, S. Grab, Phys. Lett. **B679** (2009) 45-50. [arXiv:0811.0200 [hep-ph]].
  - [29] H. K. Dreiner, S. Grab, T. Stefaniak, [arXiv:1102.3189 [hep-ph]].
  - [30] Y. Kao and T. Takeuchi, arXiv:0910.4980 [hep-ph].
  - [31] B. C. Allanach, A. Dedes and H. K. Dreiner, Phys. Rev. D **60** (1999) 075014 [arXiv:hep-ph/9906209].
  - [32] B. Malaescu, arXiv:1006.4739 [hep-ph].
  - [33] D. Stockinger, arXiv:0710.2429 [hep-ph].
  - [34] The Heavy Flavor Averaging Group *et al.*, arXiv:1010.1589 [hep-ex].
  - [35] M. J. Morello [CDF and D0 Collaboration], arXiv:0912.2446 [hep-ex]; CDF Collaboration, Public Note 9892.
  - [36] S. Schael *et al.* [ALEPH Collaboration and DELPHI Collaboration and L3 Collaboration and OPAL Collaboration and LEP Working Group for Higgs Boson Searches], Eur. Phys. J. C **47** (2006) 547 [arXiv:hep-ex/0602042].
  - [37] S. Heinemeyer, W. Hollik and G. Weiglein, Comput. Phys. Commun. **124** (2000) 76 [arXiv:hep-ph/9812320]; S. Heinemeyer, W. Hollik and G. Weiglein, Eur. Phys. J. C **9** (1999) 343 [arXiv:hep-ph/9812472]; G. Degrandi, S. Heinemeyer, W. Hollik, P. Slavich and G. Weiglein, Eur. Phys. J. C **28** (2003) 133 [arXiv:hep-ph/0212020]; M. Frank, T. Hahn, S. Heinemeyer, W. Hollik, H. Rzehak and G. Weiglein, JHEP **0702** (2007) 047 [arXiv:hep-ph/0611326].
  - [38] P. Bechtle, O. Brein, S. Heinemeyer, G. Weiglein and K. E. Williams, Comput. Phys. Commun. **181** (2010) 138 [arXiv:0811.4169 [hep-ph]]; P. Bechtle, O. Brein, S. Heinemeyer, G. Weiglein and K. E. Williams, arXiv:1102.1898 [hep-ph].
  - [39] B. C. Allanach, Comput. Phys. Commun. **143**, 305 (2002) [arXiv:hep-ph/0104145].
  - [40] B. C. Allanach and M. A. Bernhardt, Comput. Phys. Commun. **181**, 232 (2010) [arXiv:0903.1805 [hep-ph]].
  - [41] G. Belanger, F. Boudjema, A. Pukhov and A. Semenov, Comput. Phys. Commun. **180** (2009) 747 [arXiv:0803.2360 [hep-ph]].
  - [42] K. Desch, H. K. Dreiner, S. Fleischmann, S. Grab and P. Wienemann, arXiv:1008.1580 [hep-ph].
  - [43] H. K. Dreiner, H. E. Haber and S. P. Martin, Phys. Rept. **494** (2010) 1 [arXiv:0812.1594 [hep-ph]].
  - [44] A. Abulencia *et al.* [CDF Collaboration], Phys. Rev. Lett. **98** (2007) 221803 [arXiv:hep-ex/0702051].
  - [45] T. Aaltonen *et al.* [CDF Collaboration], Phys. Rev. Lett. **99** (2007) 191806 [arXiv:0707.2362 [hep-ex]].
  - [46] V. M. Abazov *et al.* [D0 Collaboration], Phys. Lett. B **638**, 441 (2006) [arXiv:hep-ex/0605005].
  - [47] V. M. Abazov *et al.* [D0 Collaboration], Phys. Rev. Lett. **97**, 111801 (2006) [arXiv:hep-ex/0605010].
  - [48] W. Beenakker, M. Klasen, M. Krämer, T. Plehn, M. Spira and P. M. Zerwas, Phys. Rev. Lett. **83**, 3780 (1999) [Erratum-ibid. **100**, 029901 (2008)] [arXiv:hep-ph/9906298].
  - [49] G. J. Feldman and R. D. Cousins, Phys. Rev. D **57** (1998) 3873 [arXiv:physics/9711021].
  - [50] M. Cacciari and G. P. Salam, Phys. Lett. B **641**, 57 (2006) [arXiv:hep-ph/0512210].
  - [51] M. Cacciari, G. P. Salam and G. Soyez, <http://www.lpthe.jussieu.fr/~salam/fastjet/>.
  - [52] F. E. Paige, S. D. Protopopescu, H. Baer and X. Tata, arXiv:hep-ph/0312045.
  - [53] G. Corcella *et al.*, JHEP **0101**, 010 (2001) [arXiv:hep-ph/0011363].
  - [54] G. Corcella *et al.*, arXiv:hep-ph/0210213.
  - [55] S. Moretti, K. Odagiri, P. Richardson, M. H. Seymour and B. R. Webber, JHEP **0204**, 028 (2002) [arXiv:hep-ph/0204123].
  - [56] W. Beenakker, R. Hopker, M. Spira and P. M. Zerwas, Nucl. Phys. B **492** (1997) 51 [arXiv:hep-ph/9610490]; W. Beenakker, M. Krämer, T. Plehn, M. Spira and P. M. Zerwas, Nucl. Phys. B **515** (1998) 3 [arXiv:hep-ph/9710451]; W. Beenakker, S. Brensing, M. Krämer, A. Kulesza, E. Laenen and I. Niessen, JHEP **1008** (2010) 098 [arXiv:1006.4771 [hep-ph]]; S. Bornhauser, M. Drees, H. K. Dreiner, J. S. Kim, Phys. Rev. **D76** (2007) 095020. [arXiv:0709.2544 [hep-ph]]; W. Hollik, M. Kollar, M. K. Trenkel, JHEP **0802** (2008) 018. [arXiv:0712.0287 [hep-ph]]; W. Hollik, E. Mirabella, M. K. Trenkel, JHEP **0902** (2009) 002. [arXiv:0810.1044 [hep-ph]]; H. K. Dreiner, S. Grab, M. Krämer, M. K. Trenkel, Phys. Rev. **D75** (2007) 035003. [hep-ph/0611195].
  - [57] Rene Brun and Fons Rademakers, Proceedings AIHENP'96 Workshop, Lausanne, Sep. 1996, Nucl. Inst. & Meth. in Phys. Res. A **389** (1997) 81-86. See also <http://root.cern.ch/>.
  - [58] C. Amsler *et al.* [Particle Data Group], Phys. Lett. B **667** (2008) 1.